

Effects of spin-phonon interaction on the properties of in high- T_C superconductors.

T. Jarlborg

Département de Physique de la Matière Condensée, Université de Genève, 24 Quai Ernest Ansermet, CH-1211 Genève 4, Switzerland

(March 24, 2018)

The mechanism of spin-phonon coupling (SPC) in high- T_C copper oxides is explored from band calculations on $\text{La}_{(2-x)}\text{Sr}_x\text{CuO}_4$ and $\text{HgBa}_2\text{CuO}_4$ systems. The LMTO band calculations, based on the local density approximation, are made for cells containing frozen phonon displacements and/or spin waves within the CuO plane. The virtual crystal approximation is used for studies of hole doped systems. The main result is that phonons are favorable for spin waves and vice-versa, and that pseudogaps appear naturally in the band structures of striped materials with strong SPC. The qualitative results are compatible with many observations showing that the properties of high- T_C superconductors depend both on lattice interactions and magnetic fluctuations. The band results are used to model various properties, mainly of the normal state, such as isotope effects, pseudogaps, Fermi surface broadening, T-dependence of the pseudogap, phonon softening and some aspects of superconductivity. The possibility of perpendicular SPC is investigated, partly by the use of a nearly free electron model.

I. INTRODUCTION.

Extensive experimental studies of high- T_C materials have been able to determine a phase-diagram for hole and electron doped members of the cuprates. Undoped materials are anti-ferromagnetic (AFM) insulators, where every second Cu along $[1,0,0]$ has opposite spin. Superconductivity on the hole doped side appears for x , the number of holes per Cu, being approximately between 0.05 and 0.25, with a maximum of T_C for $x \approx 0.15$ ¹. A pseudo-gap appears below a temperature T^* which is considerably larger than T_C when x is lower ("underdoped") than that of optimal T_C ². The width of this gap is fairly constant up to T^* , where it disappears quickly. Magnetic moments are detected in AFM fluctuations as shown from studies by neutrons³. Side peaks seen in neutron scattering suggests that the basic AFM correlation is modulated with different periodicity as the doping is changing up to a maximum x ³. Static or dynamic stripe structures appear as regions of different spin and charge along the CuO bond direction ($[1,0,0]$ or $[0,1,0]$). Results from angular resolved photoemission (ARPES), taken at low T, indicate that the cylindrical M-centred Fermi Surface (FS) "disappears" near the crossing with the X-M or Y-M lines in underdoped cases, while the band crossing on the $[1,1,0]$ line persists as a "FS-arc"⁴. The lattice is

also influenced by doping so that oxygen phonon modes become softer as the doping is increased⁵⁻⁷. More evidence of the importance of lattice interaction comes from studies of isotope effects, such as on T_C , where the effect is rather weak, on T^* , on the penetration depth⁸⁻¹⁵ and recently on the peak structures seen in photoemission¹⁶.

On the theoretical side the problem with local-density band calculations is that they do not find the AFM insulating ground state of the undoped systems. The calculated ground state is metallic and non-magnetic, but the FS compare well with positron annihilation experiments for the doped cuprates^{17,18}.

These and other features need to be understood in the complex physics of high- T_C cuprates. The present study of properties high- T_C physics is based on electronic structure calculations for hole doped supercells of two of the simpler copper oxide materials, $\text{HgBa}_2\text{CuO}_4$ (HBCO) and $\text{La}_{(2-x)}\text{Sr}_x\text{CuO}_4$ (LSCO). The Fermi surfaces (FS) of these two cuprates contain only the M-centred barrel-like cylinder, which originates from the 2-dimensional CuO -planes. Other smaller FS-pockets or ridges are found in the more complex high- T_C materials¹⁹, but it is probable that superconductivity is localized to the barrels, since they are common to all of the high- T_C cuprates.

Section II describes the band calculations and the main results. In section III is presented different models, based on SPC and the results of the band calculations, for different properties of the high- T_C cuprates.

II. BAND CALCULATIONS.

A. Method of calculation.

Electronic structure calculations, based on the local density approximation, LDA²⁰ and the Linear Muffin-Tin Orbital (LMTO) method^{21,22} are used to determine the bands for unit cells of different size and doping. Hole doping is introduced via the virtual crystal approximation, in which electrons and nuclear charges on La are reduced in LSCO. In HBCO the reduction of electronic charge is compensated by reducing the nuclear charges about equally on Cu and O sites. The the effect of disorder due to local La-Sr substitutions or interstitial O doping is not included. The calculations for HBCO include empty spheres (5 per formula unit, f.u.) in the open part of the cells. No empty spheres are introduced in the structures of LSCO. Larger supercells were considered for LSCO (7 sites per f.u.) than for HBCO (13

sites per f.u.). The supercells include phonon displacements of oxygens in the CuO plane and/or spin waves with moments on Cu sites. The stacking sequence along \hat{z} is tetragonal for HBCO ([0,0,z]), while in LSCO it is body centered tetragonal ([0.5,0.5,z]). The present work does not investigate the coupling between different CuO planes. The bands near E_F in the calculations for the 1 f.u. cells agree well with other calculations.

Other details of the band calculations and some results on SPC can be found in previous publications^{23–27}. It can be anticipated from the nearly-free-electron (NFE) model that gaps appear at zone-boundaries $G/2$ because of small potential perturbations V_G ^{28,23}. This has been confirmed in band calculations on $\text{HgBa}_2\text{CuO}_4$, when the potential has modulations along [1,1,0] or [1,0,0] in the CuO-plane because of atomic displacements²³. Atomic displacements of the planar O-atoms on both sides of a Cu-atom are alternatively displaced towards ("compressed") or away from the Cu ("expanded"). Calculations with anti-ferromagnetic (AFM) field on the Cu atoms are made to model spin-waves. It is assumed that adiabatic conditions exist, so that the electronic time scale is much shorter than that of phonons. Only relatively slow spin waves are of interest here, when the time scale of spin waves is of the same order as for phonons. In this case one can perform "frozen" spin-wave and "frozen" phonon calculations.

B. Parallel coupling.

When the calculations are made for coexisting phonon and spin waves, it turns out that the magnetic moments are largest on the "expanded" Cu-sites. The nodes of modulated spin waves are chosen to coincide with "compressed" Cu-sites. Figure 1 shows the CuO plane containing a phonon distortion and the spin wave, both oriented along the CuO bond direction, [1,0,0]. The phonon mode creates a potential modulation of the Coulomb potential (a Fourier component V_G). Spin waves induce a modulation in the spin-polarized part of the potential and magnetic moments on the Cu. Gaps appear at different energies depending on the wave length of the modulation. The gain in kinetic energy is maximized when the gap is at E_F , which leads to a correlation between wavelength, E_F and doping. The wavelength of the spin wave is twice that of the phonon, because the spin can be up or down at "expanded" Cu-positions. The bands show two gaps for modulations along [1,1,0], one due to the phonon and one at a higher energy because of the spin wave, and there is no direct SPC for electrons at E_F . However, for modulations along [1,0,0] two rows of CuO exist along the unit cell, and the phase of the spin wave along each row differ by π . The band results show in this case a constructive SPC, where the gap from separate phonon and AFM-modulations will open a gap at the same energy, i.e. at E_F for the correct doping. In

addition, a phonon with large atomic displacements will increase the moments along the spin wave and the size of the gap. This situation reminds of a (dynamic) Peierls state, although it is not necessary that E_F coincides with a peak in the density-of-states (DOS).

Several calculations have been made where partial gaps appear at E_F for different doping levels for HBCO and LSCO with different wave length (periodicity) of phonons and/or spin waves. Large cells, containing from 56 to 224 sites, are used for studies of long periodicities, and the number of k-points are reduced accordingly (48 to 18 points in the irreducible zone). Sometimes this introduces structures in the DOS even when the cell contain no wave. To search for partial gaps it is necessary to compare the DOS functions between cases with and without phonon and/or spin waves, and in some cases also when phonon or spin amplitudes are different.

In figure 2 is shown one typical example of DOS and partial gaps. These DOS functions are calculated for 16 f.u. (112-sites) cells of LSCO, extended 8 f.u. along [1,0,0] (twice as long as in fig. 1) and 2 f.u. along [0,1,0], and the DOS for the normal 1 f.u. cell is shown for comparison. The periodicity of the spin and/or O-phonon wave along [1,0,0] makes a dip in the DOS at E_F for a doping of 4 holes per cell, i.e. for $x=0.25$. A shorter cell, as in fig 1, opens the gap at lower energy relative to E_F^0 , the position of E_F in undoped LSCO, at 0.5 holes per Cu. The longer the periodicity is the smaller doping is needed for having the gap at E_F . Infinite periodicity corresponds to undoped systems. It is often seen that weaker gaps appear symmetrically above the position of E_F^0 , suggesting that partial gaps should appear also in electron doped cases.

An effort to study the dependence of the partial gap as a function of the wave length has been done for LSCO using 4, 8 and 16 cells in the [1,0,0] direction. With always $2a_0$ along [0,1,0] and 7 sites per cell, this implies calculations with 56 (as in fig.1), 112 and 224 atoms per unit cell. The difficulty is to have a smooth DOS for the longest unit cells with only a limited number of k-points. In table I is shown the maximal deviation of charge on Cu-sites, ΔQ , for calculations with a phonon distortion along the cells. The distortions are $0.02a_0$ on the oxygens between the Cu sites in all cases, see fig. 1 for the cell of length $4a_0$. The distortions are "step-like" (not sinusoidal) for the longer cells. The result is that the maximal deviation of Cu charges increases with the length of the cell, i.e. a long phonon wavelength imply a strong charge modulation, a large potential perturbation and a large gap. Spin-polarized calculations for "step-like" modulated spin waves within the same structures, where magnetic fields of ± 10 mRy are applied on the Cu-sites, give a distribution of magnetic moments on the Cu sites. The moments are zero on two node positions with a maximal amplitude far from the node in the interior of a magnetic stripe. The maximal amplitudes are shown in Table I, and it is seen that the cell with the intermediate length has the largest moments. The SPC

seems less effective for the longest cell. The shortest cell also has low moments because there is only one row of magnetic Cu between the nodes, while in the intermediate case there are three rows of magnetic Cu sites. If the results based on these three cases are correct, one can conclude the following: The SPC is optimal for the wave of intermediate length, while for less doping and longer wavelengths the phonon distortions become relatively more important. But the interpretation can be different if perpendicular coupling is considered.

The results of the ab-initio calculations for frozen spin-phonon waves have to be reinterpreted for the real case of dynamic waves, where the partial gaps are less visible. The idea is that SPC waves exist below a certain temperature (T^*) (see later). The spin wave is the most important of the two waves for the gap, but it needs the phonon displacements to develop and it is quenched above T^* . This scenario is not proven through ab-initio calculations of total energies, but models in the following sections are used for a qualitative account of the expected properties of such a mechanism.

C. Perpendicular coupling.

It was concluded above that magnetic fluctuations are enforced on Cu when oxygens are moved away from the Cu, as is depicted in fig. 1. The first column of Cu atoms (site 1 and 2) and the third column (site 5 and 6) have large moments because there is more space around them. Zero moment nodes are on the second and fourth columns of Cu, to produce a spin-wave modulation in the rows along \hat{x} . It can be argued that spin waves are also possible along \hat{y} on the first and third columns of fig. 1. Coupling with phonons along \hat{y} is likely too. The wavelengths along columns and rows need not to be equal. This type of perpendicular spin-phonon coupling will generate double gaps in the DOS. A possible arrangement of spin wave and phonon configurations is shown in figure 3, where the simple cell in figure 1 is turned vertically and repeated four times horizontally. A short wavelength modulation along \hat{y} in fig. 3, coexists with a twice as long spin wave along \hat{x} . This is about the smallest possible cell for complete spin waves and phonons. It requires 224 atomic sites for LCSO (or 416 for HBCO), which is a bit large for well converged ab-initio calculations. In fig 4 is shown the DOS for a truncated cell, half as large along \hat{x} and \hat{y} as the cell in fig. 3. A single phonon is oriented along \hat{y} and a spin wave along \hat{x} . The number of k-points is insufficient for a smooth DOS, but the figure shows that two gaps emerge simultaneously as function of the strength of the spin wave. The two gaps are found at the expected positions for waves of these lengths along \hat{x} and \hat{y} . The gap at low energy is due to the short wave along \hat{y} , while a second partial gap develops at higher energy because of a longer spin wave along \hat{x} . In figure 5 is shown the DOS for two

different amplitudes of the phonon distortion, but with the same strength of the spin wave. Again, it is found that both gaps appear to be stronger if the strength of one of the waves becomes stronger.

These results indicate that the SPC can be mediated between perpendicular directions, to produce double gap features in the DOS. It is assumed that the gaps exist in the normal state below T^* , although they should be easiest to observe at low T.

The doping dependence of two gaps in BSCCO observed from tunneling below T_C by Zasadinski et. al.²⁹ suggests, together with the mechanism of perpendicular SPC, that the lower gap is always at a fixed energy relative to E_F^0 . However, the main upper gap moves downwards, i.e. closer to the low energy gap when the doping increases. In other words, there are fewer states between the two gaps at large doping. The calculated DOS for one cell of $\text{HgBa}_2\text{CuO}_4$, shown in fig. 6, is ranging from 11 to 20 states per Ry and CuO unit in the relevant energy region. A doping of 0.25 holes/Cu corresponds to a SPC wave of $8a_0$, twice as long as in fig. 1. (The band results can be summarized in the relation $\Lambda = 2/x$, where the doping x is in units of holes/Cu and the wavelength Λ is in units of a_0 .) A SPC wave of this length, consisting of three rows of AFM Cu plus one nonmagnetic Cu on a node position, is often visualized, since it would give the satellite peaks in neutron scattering³.

The result gives an estimation of the position of the lower gap; about 20 mRy below a reference given by E_F^0 , see fig. 6. With dopings 0.1 and 0.15 holes per Cu, the main gaps should be at 9 or 13 mRy below the reference. Thus, the separation of the two gaps is about 7 mRy (100 meV) for 0.15 holes/Cu and about 11 mRy (150 meV) for 0.1 holes/Cu, respectively. These cases correspond to wavelengths of ~ 13 and $\sim 20a_0$ perpendicular to the one at $8a_0$. In the tunneling spectra of ref.²⁹ for optimally doped and underdoped BSCCO, the energy separations are 100 and 140 meV, respectively. Such values fit reasonably well to the assumed perpendicular wave lengths at the correct values of doping (0.15 and 0.1 holes per Cu). The overdoped sample in ref.²⁹, showing a separation of about 60 meV, can be interpreted as a result of a doping of about 0.19 holes/Cu and a perpendicular wave of length $10a_0$.

A similar analysis based on the calculated DOS of La_2CuO_4 gives smaller energy separations since the DOS is larger (16-25 states per Cu), and E_F is shifted relative to the van-Hove singularity. Thus the DOS peak is at 0.15 instead of at 0.25 holes per Cu, as shown in fig. 6 for $\text{HgBa}_2\text{CuO}_4$.

From these results it is now possible to propose another conclusion about the SPC and the length of the phonon and spin wave: Since the intermediate length ($8a_0$ containing 2 phonon waves and one spin wave) show the largest SPC (cf. Table I), it can occur along some direction (\hat{x}) for all dopings. This would fit into the observations of saturated side peaks in neutron scattering for doping larger than about 0.15. The additional spacing

around Cu within the magnetic stripe (the middle row of three magnetic ones) will bring those Cu sites close to the critical point for a magnetic instability, and these sites may participate in modulated spin waves along \hat{y} . The latter waves can still be assisted by phonon distortions. If the gap from the longest wave produce the deepest gap, it will be adjusted to the position of E_F . The two gaps will merge when the doping approaches 0.25 and the two directions have similar waves.

Band calculations are too tedious for very large cells containing perpendicular spin-phonon waves of realistic length. The discussion above is based on extrapolations. From the mechanism of perpendicular SPC, it is expected that the waves come in units of $2a_0$, as in the idealized band calculations. Imperfections, twinning and dynamic effects etc., lead to incommensurate wave lengths in real materials. It is also clear that the calculated gaps for frozen configurations are deeper than averaged gaps from dynamic waves.

D. SPC along $[1,1,0]$ and nickelates.

Calculations of SPC along $[1,1,0]$ showed that the gaps from the two waves appear at different energies. Calculations have not been done for the nickelates, but neutron scattering has found that charge- and spin-strips are oriented along $[1,1,0]$ ³. The results for waves along this directions can therefore be used to interpret the result for the nickelates. Two gaps in the DOS are expected, but the difference in energy is fixed by the factor of two of the wave lengths of parallel spin and phonon waves. This is in contrast to the variable energy difference between the two gaps induced by perpendicular coupling. This prediction from SPC suggest studies also of nickelates through APRES and STM measurements. The correlation between incommensurability ϵ (the inverse of the wave length) and doping is found to be approximately linear for hole doping between 0.0 and 0.5 in the nickelates³. This is as the results for the SPC calculations along $[1,1,0]$ of the cuprates²³. Since the gaps of spin waves and phonons appear at different energies there is no constructive SPC, and this might explain why the nickelates are not superconductors.

The model of SPC predicts different behavior of double gap structures for waves oriented along $[1,1,0]$. At least if perpendicular SPC is excluded. The band calculations for HBCO showed that two waves (spin and phonons) along $[1,1,0]$ will open gaps at different energies²³. The relation between hole doping x and wavelength W (still in units of a_0) is $x = \sqrt{2}/W$. This means that a long ($W = \sqrt{2}n$) supercell with n unit cells oriented along $[1,1,0]$, will have one gap (because of the spin wave) at an energy where the total cell contains xn holes, and a second gap (because of the shorter phonon wave) at a lower energy where the doping should have been $2xn$. The factor of two between the wave lengths of the two waves makes a

difference of 2 electrons per supercell. In other words, the DOS per supercell can harbor two electrons between the two gaps. This leads to relatively close gaps for small doping levels and wider energy separation as the doping increases, which is in contrast to the observed trend on the cuprate²⁹.

Neutron data find modulations along $[1,1,0]$ also for the cuprate, but only for the lowest doping. For $x \geq 0.05$ the modulations occur along $[1,0,0]$, and there is a linear relation between x and ϵ for x approximately between 0.05 and 0.15³. For x larger than 0.15 there seems to be a saturation, with a nearly constant ϵ . This behavior is compatible with perpendicular SPC when no waves shorter than $4a_0$ (i.e. $8a_0$ for the spin wave) are possible. Calculations of total energies have not been attempted for comparisons of waves along the two directions. But a simple qualitative reason for the crossover from $[1,0,0]$ to $[1,1,0]$ at some low doping can be found from the rigid-band variation of the Fermi surface of HBCO²³. The FS for the undoped case is a M-centered cylinder with slightly larger band dispersions at the FS-crossings between Γ and M than between X and M , see fig 2 of ref.²³. The radius of the cylinder increases with doping and the FS will reach the X -point, where a van Hove singularity is formed for $x = 0.25$ per Cu. This means that there are increasingly more states near the X -point for increasing doping. A wave oriented along $[1,0,0]$ will open a gap mostly for states near this point (see also the NFE-model), which makes a large gain in kinetic energy. For less doping, when the FS is more like a perfect cylinder, there is a uniform distribution of states around the FS. Hence, there is no argument for a larger gain of kinetic energy by opening a gap along $[1,0,0]$ than along $[1,1,0]$.

The switching between waves along the CuO bond direction or along the diagonal direction presents possibilities for tests of the SPC model. A secondary gap, which is associated with T^* for SPC-waves in the bond direction, will change below $x \sim 0.05$ when the wave turns to the $[1,1,0]$ direction. The FS-smearing near the X -point at low T will also change at the critical doping. A description of the bands of nickelates from a rigid-band model based on cuprate bands puts E_F on the edge of the high DOS region. Full band calculations of the nickelates might be necessary to sort out if the arguments for the cuprates can be carried over to the nickelates, or if the change of FS will bring out very a different behavior of the physical properties.

E. Modified LDA

The AFM susceptibility are found to be stronger when a small correction to the band structure is introduced, which affects the potential and the localization. Results for the doped and undoped HBCO system have been published elsewhere²⁶. These calculations are still using

LSDA, but the LMTO linearization energies are chosen to be near the bottom of the main bands. By doing so it is found that undoped HBCO has an AFM ground state and a gap at E_F , and the undoped case show an enhancement of SPC. This result shows that a relatively small correction to LSDA can lead to a very different ground state²⁶.

The same type of correction has a similar effect on the band results for undoped and doped LSCO. Figures 7-8 show the DOS and bands for a cell of two f.u. of paramagnetic and AFM (without magnetic field) LSCO, in which anomalous linearization energies are chosen in order to promote the AFM state, as was explained above for HBCO. The highest occupied band along the $\Gamma - X$ line is susceptible to have band gaps, if potential perturbations V_G are present, as in the nearly-free-electron model. When doping is considered in a modulated cell as in fig. 1, it gives larger coupling parameters λ_{sf} for spin fluctuations. The same trend was found for HBCO, where λ_{sf} was increased from about 0.2 in normal LDA to 0.5 in the adjusted case²⁶.

III. MODELS FROM BAND RESULTS.

A. Phonon softening.

A phonon which is accompanied by a spin wave will open a partial gap at E_F . The idea is to estimate the phonon softening through the gain in kinetic energy caused by the gap.

The displacement amplitude u of atomic vibrations is in the harmonic approximation given by^{30,19}

$$u^2 = 3k_B T / K \quad (1)$$

at high T, and

$$u^2 = 3\hbar\omega / 2K \quad (2)$$

at low T. The force constant $K = M\omega^2$, where M is the atomic mass and ω is the vibration frequency, can also be calculated from the second derivative of the total energy E_{tot} , $K = d^2 E_{tot} / du^2$. From the latter relation it is expected that K should be independent of the mass. The crossover from the low-T value of u^2 , which is due to zero-point motion, to the high-T value is approximately given by $\hbar\omega / k_B$. The value of K is typically 25 eV/Å² for an O phonon with $\hbar\omega \sim 80$ meV, which makes u about 0.06 Å at room temperature. The sum of elastic energy $U = 0.5Ku^2$ and the kinetic energy $W = 0.5M\dot{u}^2$ is constant in time for harmonic vibrations. Spin waves can, in analogy with phonons, be assigned a magnetic moment $m^2 = k_B T / K_m$, where $K_m = d^2 E_{tot} / dm^2$. The band results showed that m is larger when u is large, and $m \approx 0.3 \mu_B / \text{Cu}$ at room temperature for the coexisting phonon and spin waves. A partial gap at E_F removes roughly half of the DOS within an energy $\Delta = 100$ meV around

E_F , which leads to a gain in kinetic energy; $\frac{1}{2}N\Delta^2 = 8$ meV/Cu, i.e. about 15-20 percent of the elastic energy $U = \frac{1}{2}K \cdot u^2$ for a typical u . Thus, the phonon energy is expected to decrease by the this percentage because of the coupling to the spin wave, but only in the doped case when E_F is at the gap. These results are only indicative, but they compare reasonably well with experiment^{5,6}.

The bond-stretching mode at the zone boundary is the perfect mode for this effect. But the bond-stretching movements are involved also for modes with shorter q -vectors, so the softening can occur for less doping. Since the result depend on a partial gap at E_F , it is expected that the softening should be weaker when $T \rightarrow T^*$.

B. Isotope effects.

Isotope effects (IE) on various properties have been measured on several high- T_C oxides by use of different techniques and different types for the crystal growth^{8,9,16}. As will be discussed, many problems of interpretation will be encountered when analyzing the isotope effect. The isotope effect on T_C is briefly discussed in the section about superconductivity.

The usual IE is caused by the change in vibration frequencies when the isotopes are exchanged. With SPC there is an additional effect coming from the change in vibration amplitude. The zero-point motion makes a mass (M) dependence $u \sim (K \cdot M)^{-1/4}$, and the frequency depends as $(M)^{-1/2}$ for a constant K . However, contrary to the case of simple harmonic vibrations, a small M will decrease K because spin waves are promoted when u is larger. This makes isotope effects larger than what is suggested from a constant K . The effect on the pseudogap will be moderated at large T, when there is no explicit mass dependence of u , $u^2 \sim K^{-1}$. Anharmonic effects are expected to mix phonon and spin contributions.

Several measurements of the IE on the pseudogap has been published¹²⁻¹⁴. The methods determine the transition temperature through the changes in properties obtained from NQR relaxation¹⁴, increase of linewidth from crystal field transitions observed in neutron scattering¹³, XANES experiments¹⁵, or Muon spin rotation¹². These methods provide indirect measurements of T^* , and the results depend on the rapidity of the probe. The conclusion from several measurements of the Zurich group is that a heavier oxygen isotope leads to a substantial increase of T^* , more than the effect on T_C ¹⁰⁻¹³. Direct observations of the DOS peaks below the pseudogap has been observed recently through angle-resolved photoemission, ARPES¹⁶.

The mechanism of SPC is compatible with the ARPES results for the IE in optimally doped Bi2212 where samples of equal doping with O¹⁶ and O¹⁸ are used¹⁶. The 'incoherent' DOS peak below the pseudogap, is shifted upwards, towards E_F , for the sample with the heavy isotope. Thus, a pseudogap is narrower for large O-mass,

as is expected from the diminished vibration amplitude for heavy atoms and weaker spin fluctuations. Calculations for HBCO show that the moment per Cu-atom increases by 30 percent when the displacement amplitudes are changed by a factor 1.5. A change of isotopes from O^{18} to O^{16} is expected to increase the phonon amplitude by about 3 percent, which roughly can be translated into an increased gap by about 2 percent. This is considerably smaller than found experimentally, however the calculated effect will be larger if the softening of the force constant K (from the spinwave) is taken into account. At larger T , of the order 100 K, Gweon et. al. finds that the isotope shift is smaller than at low T (25 K)¹⁶. This is expected from the behavior of the IE on vibration amplitude. When zero point motion is dominant at low T there is an IE on u , while at large T , when T is approaching the Debye Temperature, there is not. Since the O-modes are of high energy it is expected that some IE should remain at rather large T . These results are obtained when no special phonon softening (on K) is present.

The immediate conclusion from the same reasoning is that T^* and the gap should decrease when heavier isotopes are used. Measurements of the Cu NQR relaxation in Y124 containing O^{16} or O^{18} , find only a small IE on T_C and on the spin gap (defining T^*)¹⁴, in agreement with SPC. The relative downward shifts for both temperatures are about one percent or of the order of 1 K for the heavier isotope. However, it has been argued that the time scale of the NQR experiment is not sufficient to probe phonon vibrations¹³. The signatures of T^* from various fast probe experiments indicate that an increased mass lead to a large *increase* of T^* ^{13,12,15}. This is in contrast to what can be expected from a narrowing of the gap in the ARPES results¹⁶ and from the results of the present SPC calculations.

Various hypothesis can be put forward in order to understand this discrepancy between the measured T^* and the SPC mechanism. First, a light mass will be more itinerant than a heavy one. This can be understood from the difference in diffusion constant D , which behaves as³¹ $D \sim \omega a^2 \exp(-E_d/k_B T)$, where E_d is an energy barrier for hopping to another site. A higher hopping frequency (ω) together with a larger u (from which a barrier is easier to overcome) for a small mass, leads to larger diffusion compared to the case with a heavier mass. A light isotope can more easily reach interstitial positions than a heavy one, and thereby leave normal lattice positions vacant. This can modify the effective hole doping and therefore mask the true isotope effect. The effective doping is sensitive to many things. For example, it is often difficult to separate the true pressure dependence on T_C from indirect effects caused by the pressure such as oxygen ordering and the effective carrier concentration within the CuO-planes³². If heavier isotopes imply improved material properties, less disorder and distortion, it can make the pseudogaps sharper so that T^* appears to be larger. In fact, experimental data often show sharper transitions

with O^{18} than with O^{16} , as for the intrinsic lineshape of the crystal-field transition¹³, and in XANES data¹⁵. An indication of a better shaped gap can be found in the ARPES data for O^{18} of Gweon et. al.¹⁶, which show a shoulder in the gap coming from the so-called superstructure replica in Bi2212. The shoulder is less pronounced for O^{16} although the position of the incoherent peak indicates a wider gap.

Other explanations of the observed increase of T^* with heavy isotopes might be proposed because of the particular techniques of the different experiments. But admittedly, the present calculations of SPC provide no obvious explanation of these measurements^{13,12,15}.

The mass dependence of u is largest at low T , which suggests that measurements of the penetration depth¹⁰ Λ at low T should be good for detecting IE. Some assumptions lead to $\Lambda^{-2} \sim N \cdot v^2$, where N is the DOS at E_F and v is the Fermi velocity. The 3d average of this product will be small if a partial gap appears at E_F , and a light mass with large u makes the product even smaller ($N \rightarrow 0$ for a complete gap). This is opposite to experiments of the Zurich group^{10,11}. However, the SPC result can be different if only the planar directions of v are considered, as would be the normal ansatz for a magnetic field perpendicular to the CuO planes. The band crossing E_F along Γ -M has larger v than at the crossing along X-M. Phonon and spin waves along $[1,0,0]$ will produce the gaps in the latter region and v will increase more for the material with light isotopes. One can estimate that an increase of u by 3 percent will decrease N by 1-2 percent. As $N \sim v^{-1}$ this suggests a slight increase of Λ^{-2} .

C. T-dependence of the gap.

It is often observed, in STM for example³³, that the pseudogap remains rather intact as T increases. The peaks around the gap are at fixed positions, and they are not so much getting closer as T is approaching T^* , but the peaks are smeared. The behavior is different from that of a superconducting gap, which becomes narrower when $T \rightarrow T_C$. This suggests that the mechanism behind the pseudogap is disconnected from superconducting pairing. It can also be noted that that T^* and T_C show no scaling as function of doping, but that T^* is much larger than T_C at low doping. A sudden disappearance of the gap at a high T , can be understood if spin fluctuations, rather than phonons, are the main cause of the gap.

It can be recalled that the states below and above the gap in the NFE model are separated in real space. The lowest state for "spin up" bands in an AFM case is localized on sites where the spin polarized potential is attractive for spin up electrons. The other sites have the spin down states occupied. For $T=0$ and E_F in the gap, the low energy states are occupied, while states above E_F (which have opposite spin distribution) are unoccupied.

The separation between low and high energy states leads to a real space separation of spin up and spin down electrons. But the Fermi-Dirac (FD) distribution at high T will not separate the occupied spins below E_F from the opposite spin above E_F as much as at low T . The local magnetic moments (m) will decrease, which will decrease the spin splitting, which will decrease m further and so on. This process is modeled by use of low- T parameters of the gap Δ and m , which are compatible with the band results at low T . At $T=0$, when the FD occupation, f , is a step function there is an optimal separation between the occupied majority spins at $E_F - \Delta$ from the unoccupied minority spins at $E_F + \Delta$, and $m \approx N \cdot \Delta$, where the DOS, N , is assumed to be constant. As function of T , $m(T) = N \cdot \Delta \cdot (f(\frac{-\Delta}{k_B T}) - f(\frac{\Delta}{k_B T}))$. The result for Δ is shown in fig. 9. The reason of the rapid drop of Δ is the strong T -dependence of the FD-mediated feedback of m on Δ .

This is also exemplified for two band calculations for 8 f.u. (see fig 1) of LSCO doped with 0.5 holes per f.u.. All parameters, except for $k_B T$ in the FD-distribution, are identical. A calculation with $k_B T = 1$ mRy ($T = 158$ K) gives an AFM arrangement of local moment of $0.21 \mu_B$ on Cu, and a clear gap. When $k_B T$ is increased to 4 mRy, the moment decreases to less than $0.1 \mu_B$ after selfconsistency, and the gap is much washed out. The example is made for a very short wave, which implies large doping and low T^* . Longer unit cells corresponding to underdoped cases are required for quantitative studies of real T^* by this mechanism. Effects from thermal disorder are expected to enhance the T -dependence.

These results show the fragile nature of the magnetic state. If the gap was due to only a potential modulation from phonons, there should not be a rapid disappearance at T^* , because there is no mechanism of feedback.

Recent measurements of the optical conductivity on $\text{La}_{2-x}\text{Ba}_x\text{CuO}_4$ for $x = \frac{1}{8}$, where ordering of "charge-stripes" occurs below 60K^{34} , can be interpreted as a result of a gap in the DOS below this temperature.

D. Nearly free electron models.

Ab-initio band calculations for large unit cells are complicated. The size of the Brillouin Zone is reduced, and an unfolding of the FS to the original zone is difficult. Some insight is provided by the NFE model. A Fourier component V_Q of the potential ($V(\vec{x}) = V_Q \exp(-i\vec{Q} \cdot \vec{x})$), such as the AFM spin polarized potential of undoped cuprates, will open a gap ($2V_Q$) at $\vec{k} = \vec{Q}/2^{28,23}$. Such gaps are visible in the full band approach, see fig. 7. An additional modulation with longer wave length (wave vector $\vec{q} < \vec{Q}$), will modify the potential, $V(\vec{x}) = V_Q \exp(-i\vec{Q} \cdot \vec{x}) \exp(i\vec{q} \cdot \vec{x}) = V_Q \exp(-i(\vec{Q} - \vec{q}) \cdot \vec{x})$, and the gap moves slightly away from \vec{Q} to $\vec{Q} - \vec{q}$. The gaps in the full band approach are seen at a lower energy, see fig. 2.

By introducing a perpendicular modulation along \hat{y} , it

is possible obtain the bands from a 3 by 3 matrix with $E - k_x^2 - k_y^2$, $E - (k_x - Q_x)^2 - k_y^2$, and $E - k_x^2 - (k_y - Q_y)^2$ in the diagonal, and V_Q as non-diagonal terms. Only G-vectors 0, $\vec{Q}_x = \vec{Q} - \vec{q}$ and $\vec{Q}_y = \vec{Q} - \vec{q}'$ are considered in the basis with different \vec{q} and \vec{q}' along \hat{x} and \hat{y} . Apart from having the 2-dimensional band structure centered around Γ , the lowest bands show what is expected from the ab-initio band results in terms of band dispersion, double peaks in the DOS (if $\vec{q} \neq \vec{q}'$), and FS broadening near the zone boundaries, see figures 10-12. The k_x and k_y dispersions in fig. 10 show the partial gaps at different energies when the modulation vectors are different along the two directions, while no gap appears along the diagonal direction $[k, k]$. The FS is robust on the diagonal direction, so that an 'arc' of FS remains even with strong potential modulations, see fig. 11. Near the $\Gamma - X$ and $\Gamma - Y$ lines however, the FS will be different depending on the strength of the modulation, V_Q . A dynamic modulation will smear the FS in these areas, while the FS arc remains. This agrees with interpretations of T -dependent ARPES, where only a small section of the arc is seen at the low T^4 .

The model bands are shown for perpendicular coupling, as is motivated from the discussion of the ab-initio results. Only one gap exist if the amplitudes of \vec{q} and \vec{q}' are equal. The deepest gap in the DOS (favorable position of E_F) is for energies where the two gaps overlap as shown in fig. 12., while the smaller 'dip' appears at lower energy. Twinning and dynamic effects in real materials will mix the two directions, and the gaps will be weaker due to smearing.

E. Superconductivity.

The importance of SPC for the mechanism of superconductivity is evident, since both phonons and spin-fluctuations are mutually enhanced. A precise theory for this mechanism is still missing, but some observations can be made.

Magnetism is traditionally considered to prevent superconductivity based on electron-phonon coupling through the pair-breaking effect between electrons of opposite spins. Similarly, superconductivity mediated by spin fluctuations between electrons of equal spin is prevented by impurities or even phonons. The effect for SPC presented above, is that selected phonons create a condition for enhancement of the spin wave. Therefore, it is no longer an antagonism between the spin wave and the phonon in the case of equal spin pairing (ESP). The conditions for ESP is enhanced near the critical point for diverging magnetic susceptibility. But how this should be implemented into explicit calculations of T_C is not yet clear. In a simple BCS-like formula, $T_C \sim \omega \exp(-1/\lambda)$, λ is the coupling constant either for electron-phonon interaction (λ_{ep}) or from spin fluctuations (λ_{sf}), and the prefactor ω is the energy of the phonon or the energy of

the spin excitation, ω_p or ω_{sf} , respectively. Generally, if λ is large, then ω is small, and vice-versa. In other words, a phonon softening is about equivalent to a nearly static magnetic order, and the optimal condition for a high T_C is expected near such a transition.

From the discussion of SPC it is more probable that superconductivity is because of ESP near a critical point than because of standard electron-phonon coupling. With SPC it is possible to be very near a critical point during the cycle of a phonon vibration. The system can profit from a large λ_{sf} at the extreme phonon displacement and a reasonably large ω_{sf} when the displacements are not much developed. The SPC calculations showed that the conditions for having a pronounced spin wave are enhanced when the phonon is present, from which it can be assumed that ω_{sf} is at least not smaller than ω_p . It is possible that ω_{sf} is larger than ω_p , but as a low limit $\omega_{sf} \approx \omega_p \approx 80$ meV for O-modes. A value of λ_{sf} of the order 0.5 was calculated from the band results for a short wave in HBCO; $\lambda_{sf} = NI^2/K_m$, where $I = \int \psi^* \frac{dV}{dm} \psi d^3r$ and $K_m = d^2 E_{tot}/dm^2$ as in ref.³⁵. This gives a large value (~ 100 K) for T_C from a BCS-like formula. However, this is very indicative: The calculation of λ_{sf} is for the shortest possible wave, and the LDA potential needs corrections. Effects of the interplay between other phonon and spin waves, of Coulomb repulsion, of anharmonicity and of strong coupling are neglected.

From SPC it is quite clear that superconductivity disappears at large doping, since the limit for the wave length of a phonon is at $\frac{1}{2} \cdot 4a_0$, corresponding to $x = 0.25$ holes per Cu. Spin waves shorter than $4a_0$ has to work without (parallel) phonons. In the opposite limit, at small doping, one can see at least two reasons for the disappearance of superconductivity: First, if the mechanism of SPC and the pseudogap becomes too successful at low x , as can be deduced from the experimental trend for T^* and from some of the calculated results, it will diminish N and hence also λ_{sf} and T_C . Too strong effects from SPC implies also that either one of the waves (spin or phonon) may get too soft and become static, and thereby become inefficient for superconductivity. Another reason is the change of the wave orientation from $[1,0,0]$ to $[1,1,0]$ which is observed for $x \leq 0.05$, which in the SPC model implies the end of constructive coupling between phonons and spin waves.

The isotope effect on the superconducting $T_c \sim \omega_{sf} \cdot \exp(-1/\lambda_{sf})$ is more complex than for normal electron-phonon coupling, since λ_{sf} has an isotope effect. A pure λ_{sf} tend to increase for light isotopes because of larger displacement amplitudes. A pure phonon frequency ω_p behaves as $\sqrt{K/M}$, and above it was assumed that $\omega_{sf} \approx \omega_p$. A lower M should increase ω , but a softening of K because of SPC, will have a moderating effect. These two mass dependencies work together for a positive isotope effect as in normal electron-phonon coupling, but the total effect might be small if the phonon softening is large.

IV. CONCLUSION.

In conclusion, results from ab-initio band calculations for different configurations of spin waves and phonon distortions in HBCO and LSCO, have been used in models aimed for an understanding of various properties. At this stage, when it is not yet clear exactly which configuration is the most important one, it is preferable to make qualitative studies of a variety of properties rather than precise studies of a single effect. Thus, it has been shown that SPC leads to pseudogaps, FS broadening in the bond directions with a stable arc in between, phonon softening, and variations of the periodicity (wave length) with doping. A rapid T-dependence of the gap is consistent with rapid quenching of the spin part, while this would not be explained from phonons only. Isotope shifts are expected on many properties. Some experiments showing a strong increase of T^* for heavy isotopes are not explained, but the results are consistent with some other data showing smaller effects. The nature of SPC is such that different waves in perpendicular directions are probable. This will produce double gap structures in the DOS, as seen in the simple model of nearly free electrons. From the doping dependence of observed double peaks it is speculated that the reason this phenomenon is related to perpendicular SPC.

Quantitative, ab-initio results are difficult to obtain for very large unit cells, because of few k-points and slow convergence of total energies. The LDA ground state is too far from the AFM instability and many effects are probably underestimated in LDA. It is argued that LDA need rather modest corrections in order to promote an AFM, insulating state. The gap is in this case an ordinary band gap, caused by modulations of AFM within the CuO plane.

The results and the mechanism of SPC are sometimes very different from the conventional pictures of the physics of high- T_C superconductors. The hope is that the mechanism of SPC should give new ideas for a guidance towards the mechanism for high- T_C superconductivity.

-
- ¹ J.L. Tallon and J.W. Loram, Physica **C349**, 53, (2001).
 - ² T. Timusk and B. Statt, Rep. Prog. Phys. **62**, 61, (1999).
 - ³ J.M. Tranquada cond-matt/0512115 (2005) and references therein.
 - ⁴ M.R. Norman, H. Ding, M. Randeria, J.C. Campuzano, T. Yokoya, T. Takeuchi, T. Takahashi, T. Mochiku, K. Kadowaki, P. Guptasarma and D.G. Hinks, Nature **392**, 157, (1998).
 - ⁵ L. Pintschovius and M. Braden, Phys. Rev. **B60**, R15039, (1999).
 - ⁶ T. Fukuda, J. Mizuki, K. Ikeuchi, K. Yamada, A.Q.R. Baron and S. Tsutsui, Phys. Rev. **B71**, 060501(R), (2005).

- ⁷ H. Uchiyama, A.Q.R. Baron, S. Tsutsui, W.-Z. Hu, A. Yamamoto, S. Tajima and Y. Endoh, Phys. Rev. Lett. **92**, 107005-1, (2004).
- ⁸ G.-M. Zhao, H. Keller and K. Conder, J. Phys.: Cond. Matter, **13**, R569, (2001).
- ⁹ G.V.M. Williams, D.J. Pringle, J.L. Tallon, Phys. Rev. B **61**, R9257, (2000).
- ¹⁰ J. Hofer, K. Conder, T. Sasagawa, Guo-meng Zhao, M. Willemin, H. Keller and K.Kishio, Phys. Rev. Lett. **84**, 4192, (2000).
- ¹¹ R. Khasanov, A. Shengelaya, E. Morenzoni, K. Conder, I.M. Savic and H. Keller, J. Phys.: Cond. Matter, **16**, S4439, (2004).
- ¹² A. Shengelaya, G-M Zhao, C.M. Aegerter, K. Conder, I.M. Savic, and H. Keller, Phys. Rev. Lett. **83**, 5142, (1999).
- ¹³ D. Rubio Temprano, J.Mesot, S. Janssen, K. Conder, A. Furrer, A. Sokolov, V. Trounov, S.M. Kazakov, J. Karpinski, and K.A. Muller, Eur. Phys. J. B **19**, 5 (2001); D. Rubio Temprano, J.Mesot, S. Janssen, K. Conder, A. Furrer, H. Mutka, and K.A. Muller, Phys. Rev. Lett. **84**, 1990, (2000).
- ¹⁴ F. Raffa, T. Ohno, M. Mali, J. Roos, D. Brinkmann, K. Conder and M. Eremin, Phys. Rev. Lett. **81**, 5912, (1998).
- ¹⁵ A. Lanzara, G.-M. Zhao, N. L. Saini, A. Bianconi, K. Conder, H. Keller and K. A. Muller, J. Phys.: Cond. Matter, **11**, R541, (1999).
- ¹⁶ G.-H. Gweon, T. Sasagawa, S.Y. Zhou, J. Graf, H. Takagi, D.-H. Lee and A. Lanzara, Nature **430**, 187, (2004).
- ¹⁷ H. Haghighi, J.H. Kaiser, S. Rayner, R.N. West, J.Z. Liu, R. Shelton, R.H. Howell, F. Solar, P.A. Sterne and M.J. Fluss, Phys. Rev. Lett. **67**, 38 (1991).
- ¹⁸ A. Shukla, L. Hoffmann, A.A. Manuel, E. Walker, B. Barbiellini and M. Peter, Phys. Rev. B **51**, 6028, (1995).
- ¹⁹ T. Jarlborg and G. Santi, Physica C **329**, 243 (2000).
- ²⁰ W. Kohn and L.J. Sham, Phys. Rev. **140**, A1133, (1965); O. Gunnarsson and B.I Lundquist, Phys. Rev. B **13**, 4274, (1976).
- ²¹ O.K. Andersen, Phys. Rev. B **12**, 3060 (1975).
- ²² T. Jarlborg and G. Arbman, J. Phys. F **7**, 1635 (1977).
- ²³ T. Jarlborg, Phys. Rev. B **64**, 060507(R) (2001).
- ²⁴ T. Jarlborg, Phys. Lett A **295**, 154 (2002).
- ²⁵ T. Jarlborg, Phys. Rev. B **68**, 172501 (2003).
- ²⁶ T. Jarlborg, J. Phys.: Cond. Matter, **16**, L173, (2004).
- ²⁷ T. Jarlborg, cond-matt/0508672, (2005).
- ²⁸ J.M. Ziman, *Principles of the Theory of Solids* (Cambridge University Press, New York, (1971).
- ²⁹ J.F. Zasadzinski, L. Ozyuzer, N. Miyakawa, K.E. Gray, D.G. Hinks and C. Kendziora, Phys. Rev. Lett. **87**, 067005, (2001).
- ³⁰ G. Grimvall, "Thermophysical Properties of Materials", Ed.: E.P. Wohlfarth, North-Holland (1986).
- ³¹ C. Kittel, *Introduction to Solid State Physics* 4th edn (Wiley, 1971).
- ³² J.S. Schilling, cond-matt/0604090 (2006).
- ³³ Ø. Fischer, M. Kugler, I. Maggio-Aprile, C. Berthod, and C. Renner, Rev. Mod. Phys., (In press) (2006).
- ³⁴ C.C. Homes, S.V. Dordevic, G.D. Gu, Q. Li, T. Valla and J.M. Tranquada, cond-matt/0603763 (2006).
- ³⁵ T. Jarlborg, Physica C **385**, 513, (2003); Phys. Lett. A **300**, 518 (2002).

TABLE I. Calculated maximum deviations of charges ΔQ (el. per Cu), and moments m (μ_B per Cu) for LSCO cells of different lengths L along $[1,0,0]$. The $4a_0$ wave, is as in fig. 1, the $8a_0$ wave is like the one shown horizontally in fig. 3, and the $16a_0$ is twice as long. The cells contain phonons or spin waves with equal distortions or magnetic field per site, so that each of the distorted O-atoms is displaced $0.02a_0$ or each Cu with imposed moment has a field of ± 10 mRy.

L	$4a_0$	$8a_0$	$16a_0$
ΔQ	0.13	0.15	0.26
m	0.20	0.23	0.16

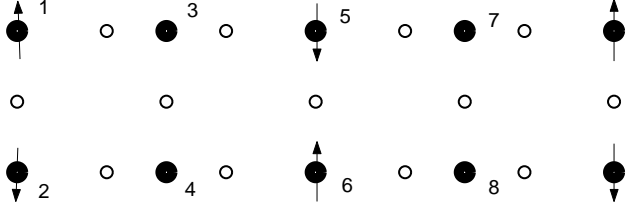


FIG. 1. The CuO plane for cells of HBCO and LSCO containing 8 f.u.. Filled and open circles indicate Cu and O, respectively, and arrows are spins. Half-breathing O-phonons are made by approaching O towards Cu in columns 2 and 4 (by $0.02 \cdot a_0$, where a_0 is the Cu-Cu distance), which will be favorable for spin moments on Cu in columns 1 and 3. The amplitude of the O-phonon displacements is exaggerated for visibility.

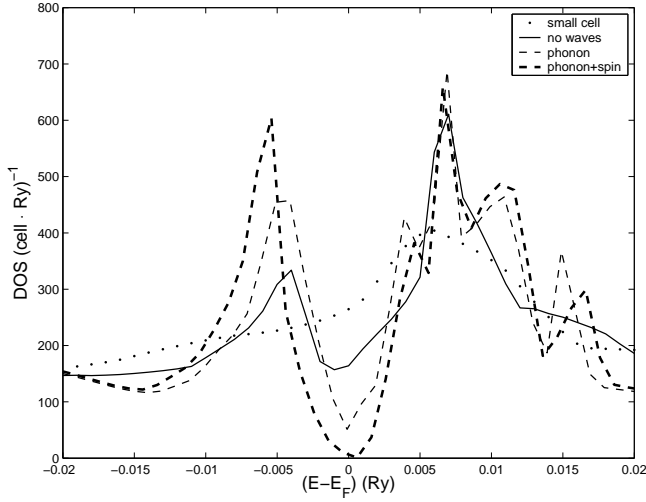


FIG. 2. DOS near E_F for a 16 f.u. cell of LSCO (twice as long as in fig. 1) of LSCO. The DOS for the 1 f.u. cell at the same doping level is shown for comparison. It is seen that the partial gap becomes stronger (deeper and wider DOS) by the phonon and the phonon plus spin wave.

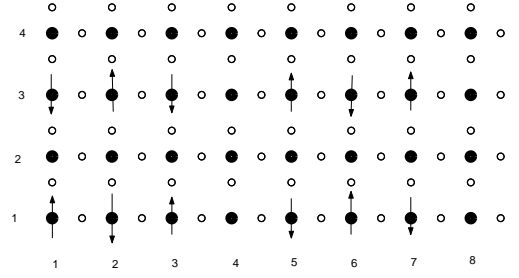


FIG. 3. The CuO plane for a large cell with different waves in perpendicular directions. Notations as in fig. 1. The dilatation around Cu in rows 1 and 3 favors spin waves within these rows. There is one coupled phonon- and spin-wave along \hat{y} (periodicity $4 a_0$) and one spin wave along \hat{x} with longer periodicity ($8 a_0$).

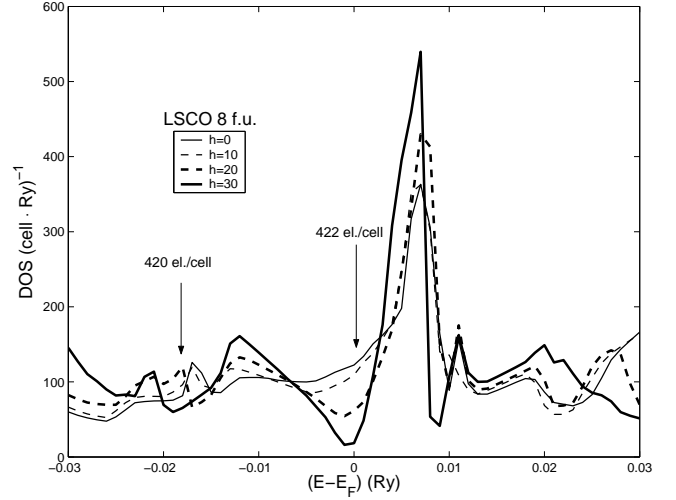


FIG. 4. AFM DOS near E_F for doped $\text{La}_{16}\text{Cu}_8\text{O}_{32}$ with phonon displacement along $[0,1,0]$ and spin waves along $[1,0,0]$ as described on the text. Two gaps become stronger for increasing magnetic field. Undoped LSCO contain 424 valence electrons per 8 f.u. cell.

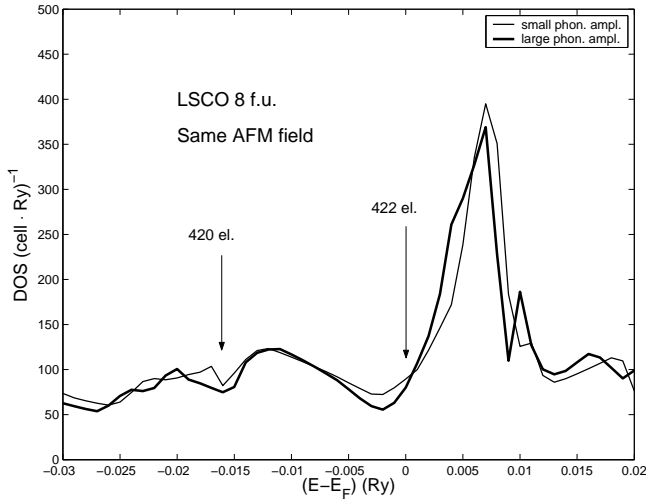


FIG. 5. AFM DOS near E_F for doped $\text{La}_{16}\text{Cu}_8\text{O}_{32}$ as in fig 4 for two amplitudes (small amplitude; thin line) of the phonon displacement.

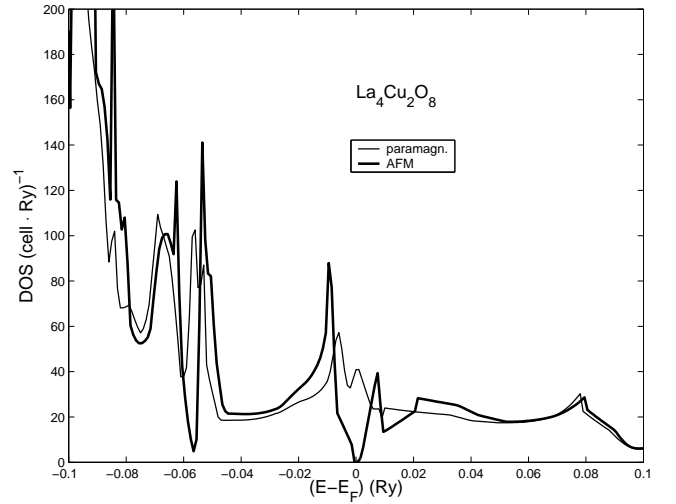


FIG. 7. Paramagnetic (thin line) and AFM (bold line) DOS near E_F of $\text{La}_4\text{Cu}_2\text{O}_8$ calculated for low linearization energies.

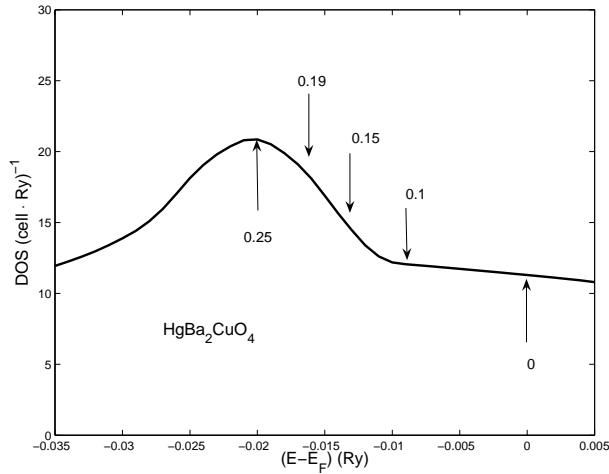


FIG. 6. The calculated DOS for one unit cell of HBCO. The arrows indicate the position of E_F as function of the number of holes per unit cell. A spin-phonon wave of length $8a_0$ will open a gap at the arrow for 0.25 holes. As is argued in the text, it is expected that a second gap will open (for less doping as indicated by the arrows) because of longer waves in the perpendicular direction. The DOS for LSCO is about 20 percent higher (see the dotted line in fig. 2), and the number of holes at the peak is 0.15.

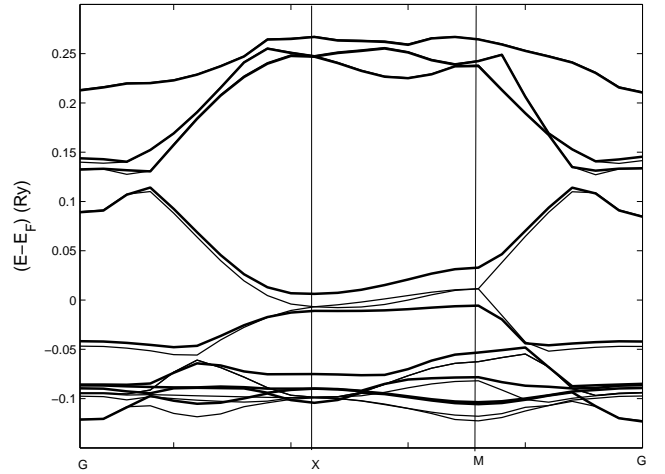


FIG. 8. Paramagnetic (thin line) and AFM (bold line) bands along the symmetry direction in the AFM Brillouin Zone for $\text{La}_4\text{Cu}_2\text{O}_8$. As in fig. 7 the bands are calculated for low linearization energies.

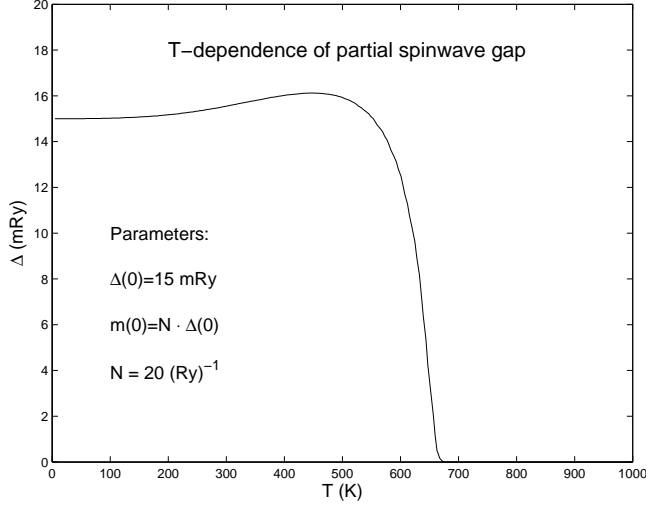


FIG. 9. A model calculation of the T-dependence of the gap parameter, Δ , caused by spin modulations. The rapid destruction of the gap at a given T is caused by the wide Fermi-Dirac occupation above that temperature and the feedback of the moment on the gap, as described in the text. The same mechanism does not work for a gap which is caused by phonons only.

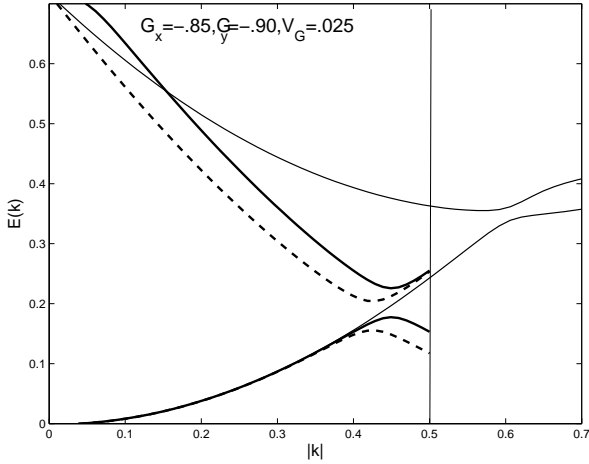


FIG. 10. The lowest bands for the 2-D NFE model with parameters corresponding to perpendicular coupling. The heavy line is along k_x , the broken line along k_y , and the thin line along the diagonal from $[0,0]$ to $[0.5,0.5]$.

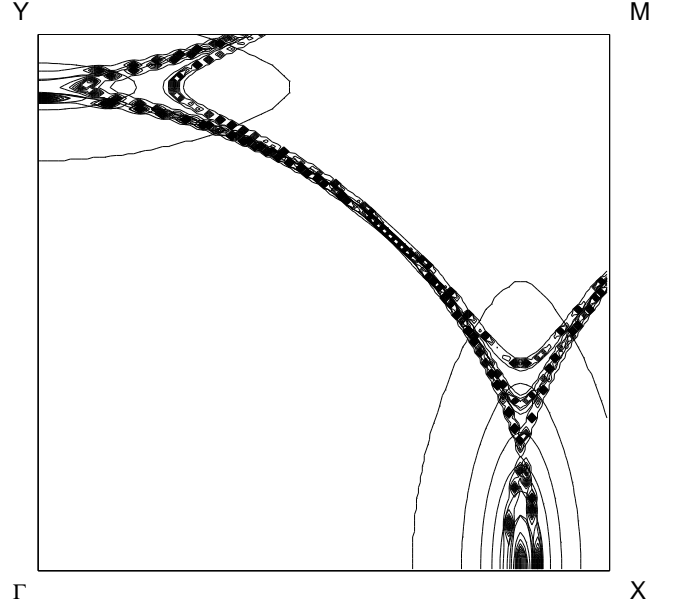


FIG. 11. The Fermi surfaces for the 2-D NFE model with three different parameters for the V_G parameter. Contour lines indicate the energy difference relative to E_F , which is chosen to be within the gap. The FS from the lowest band turns away from the $\Gamma-X$ and $\Gamma-Y$ lines, towards the $X-M$ and $Y-M$ lines, when V_G increases. The second band is close to E_F in the regions where the first band has disappeared, as is seen by the thin contours centered close to the X and Y points. Dynamical effects (or disorder and twinning) lead to FS smearing approximately within the widest contour lines, while a static case can create the 'shadow' FS crossing the $X-M$ and $Y-M$ lines. The FS-'arc', crossing the $\Gamma-M$ line, is a robust feature.

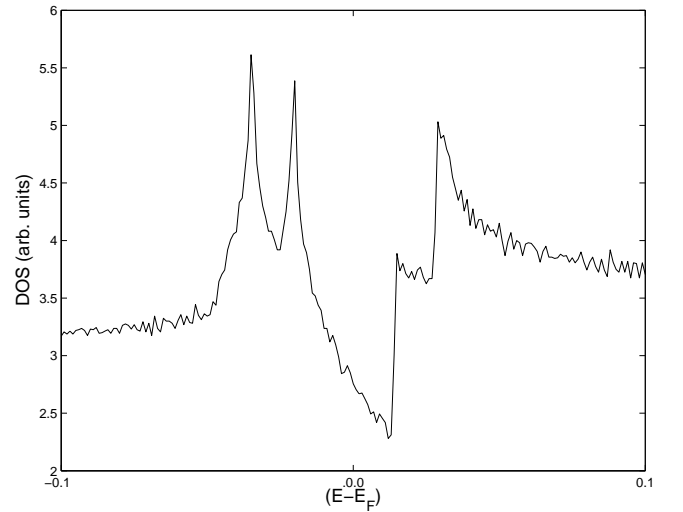


FIG. 12. An example of the DOS in 2-D NFE model with perpendicular coupling. The location of E_F is in the main gap. A smaller gap, or a 'dip', below E_F is a consequence of different gap locations along the \hat{x} and \hat{y} directions. Dynamical effects and dispersion along \hat{z} will cause smearing.